

Oxidative Addition of the Chloromethane C–Cl Bond to Pd, an *ab Initio* Benchmark and DFT Validation Study

G. Theodoor de Jong and F. Matthias Bickelhaupt*

*Afdeling Theoretische Chemie, Scheikundig Laboratorium der Vrije Universiteit,
De Boelelaan 1083, NL-1081 HV Amsterdam, The Netherlands*

Received October 14, 2005

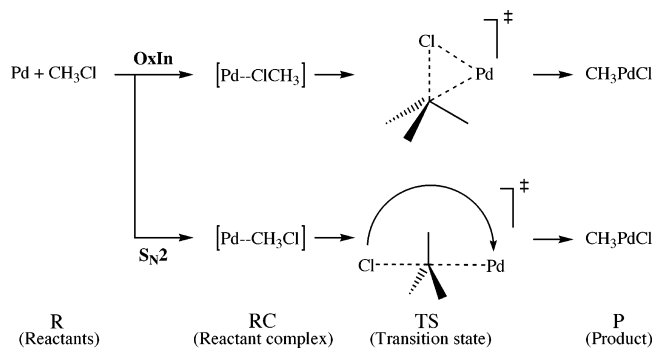
Abstract: We have computed a state-of-the-art benchmark potential energy surface (PES) for the archetypal oxidative addition of the chloromethane C–Cl bond to the palladium atom and have used this to evaluate the performance of 26 popular density functionals, covering LDA, GGA, meta-GGA, and hybrid density functionals, for describing this reaction. The *ab initio* benchmark is obtained by exploring the PES using a hierarchical series of *ab initio* methods [HF, MP2, CCSD, and CCSD(T)] in combination with a hierarchical series of seven Gaussian-type basis sets, up to g polarization. Relativistic effects are taken into account through a full four-component all-electron approach. Our best estimate of kinetic and thermodynamic parameters is -11.2 (-10.8) kcal/mol for the formation of the most stable reactant complex, 3.8 (2.7) kcal/mol for the activation energy of direct oxidative insertion (OxIn), and -28.0 (-28.8) kcal/mol for the reaction energy (all energies relative to separate reactants, zero-point vibrational energy-corrected values in parentheses). Our work highlights the importance of sufficient higher angular momentum polarization functions for correctly describing metal-d-electron correlation. The best overall agreement with our *ab initio* benchmark is obtained by functionals from all three categories, GGA, meta-GGA, and hybrid DFT, with mean absolute errors of 0.8 – 3.0 kcal/mol and errors in activation energies for OxIn ranging from 0.0 to 1.2 kcal/mol. For example, three well-known functionals, BLYP, OLYP, and B3LYP, compare very reasonably with, respectively, an underestimation of the barrier for OxIn of -4.2 kcal/mol and overestimations of 4.2 and 1.6 kcal/mol. Interestingly, all important features of the CCSD(T) benchmark potential energy surfaces for the Pd-induced activation of C–H, C–C, C–F, and C–Cl bonds are reproduced correctly within a few kcal/mol by BLYP, OLYP, and B3LYP, while at the same time, none of these functionals is the “best one” in each individual case. This follows from an overall comparison of the results of the present as well as previous studies.

1. Introduction

The catalytic activation of the C–Cl bond is an efficient tool for selectively converting simple educts, via C–C bond formation, into more complex compounds. This process, which is often based on catalytically active palladium complexes, is therefore of major importance for synthetic chemistry. The most intensively used substrates for such

C–C coupling reactions are aryl halides, whereas it is more difficult in this context to exploit alkyl halides.¹ While C–H and C–C bond activations have been the subject in various computational investigations, the oxidative addition of C–Cl or, more generally, C–halogen bonds has received less attention.² Still, there are a number of computational studies^{2–11} on the activation of C–X bonds by d^{10} metal centers, such as palladium complexes, which is one of our main subjects of interest because of its relevance for homogeneous catalysis.¹²

* Corresponding author fax: +31-20-59 87629; e-mail: fm.bickelhaupt@few.vu.nl.

Chart 1. Model Reactions and Nomenclature

Transition-metal-induced C–Cl bond activation usually proceeds via an oxidative addition process in which the metal increases its formal oxidation state by two units. There has been controversy about the mechanism of this reaction.¹³ One mechanism that has been proposed requires the concerted transfer of two electrons and involves either a concerted front-side displacement or a concerted nucleophilic displacement ($\text{S}_{\text{N}}2$) proceeding via backside attack of the C–Cl bond by the metal. Theoretical studies on the oxidative addition of the C–Cl bond in chloromethane to the Pd atom show that this process can indeed proceed via direct oxidative insertion of the metal into the C–Cl bond (OxIn) or via $\text{S}_{\text{N}}2$ substitution followed, in a concerted manner, by leaving-group rearrangement ($\text{S}_{\text{N}}2\text{-ra}$).^{3,10} The reaction barrier for OxIn is lower than that for the $\text{S}_{\text{N}}2$ pathway. Interestingly, anion assistance, for example, coordination of a chloride anion to Pd, reverses this order in activation energies and makes $\text{S}_{\text{N}}2$ the preferred pathway. Note that this shift in mechanism also corresponds to a change in stereochemistry at the carbon atom involved, namely, from retention (OxIn) to inversion of configuration ($\text{S}_{\text{N}}2$). This is of practical relevance for substrates in which the carbon atom, C^* , is asymmetric (which is obviously not the case in the simple model substrate chloromethane). The two pathways are schematically summarized in Chart 1.

The purpose of the present study is two-fold. In the first place, we wish to obtain a reliable benchmark for the potential energy surface (PES) for the oxidative addition of the C–Cl bond of chloromethane to Pd(0). This is done by exploring this PES with a hierarchical series of ab initio methods {Hartree–Fock (HF), second-order Møller–Plesset perturbation theory (MP2),¹⁴ and coupled cluster theory¹⁵ with single and double excitations (CCSD)¹⁶ and with triple excitations treated perturbatively [CCSD(T)]¹⁷} in combination with a hierarchical series of Gaussian-type basis sets of increasing flexibility and polarization (up to g functions). The basis set superposition error (BSSE) is accounted for by counterpoise correction (CPC).¹⁸ Relativistic effects are treated with a full four-component all-electron approach. To our knowledge, these are the first benchmarking calculations at an advanced correlated level for this model reaction.

The second purpose of our work is to evaluate the performance of 26 popular density functionals, covering LDA, GGA, meta-GGA, and hybrid density functionals, for describing the oxidative addition of the chloromethane C–Cl bond to Pd, using the ab initio benchmark as a reference point. Here, we anticipate that, while the latter turns out to

be satisfactory in terms of accuracy and reliability, it is prohibitively expensive if one wishes to study more realistic model catalysts and substrates. Thus, our survey of 26 density functionals serves to validate one or more of these density functional theory (DFT) approaches as a computationally more efficient alternative to high-level ab initio theory in future investigations in the field of computational catalysis.¹¹ A general concern associated with the application of DFT to the investigation of chemical reactions is its notorious tendency to underestimate activation energies.^{6,19–24} However, very recently, with the same approach as has been used in the present study, we investigated the insertion of the Pd d¹⁰ atom into the C–H bond of methane, the C–C bond of ethane, and the C–F bond of fluoromethane as important archetypal examples of oxidative addition reactions:^{25–28} DFT^{29–31} turned out to reproduce the highest level ab initio (coupled-cluster) benchmark PESs within a few kilocalories per mole.^{26–28} Interestingly, in the case of palladium-induced C–H and C–C bond activation,^{26,27} the well-known BLYP functional turned out to be among the best performing functionals, providing PESs that are better than those of most of the high-level meta-GGA and hybrid functionals. On the other hand, the activation of the C–F bond turns out to be somewhat better described by OLYP and B3LYP.²⁸ Here, we are interested in how far the same conclusions hold for palladium-induced C–Cl bond activation. In addition to evaluating and ranking the performance of the density functionals, we investigate the dependence of the resulting PES on the basis-set size and on the use of the frozen-core approximation. We conclude with a critical overview and comparison of the palladium-induced activations of all bonds for which we have so far carried out an ab initio benchmark and DFT validation study: C–H, C–C, C–F, and C–Cl.

2. Method and Computational Details

2.1. Geometries. All geometry optimizations have been done with DFT using the Amsterdam Density Functional (ADF) program.^{32–35} For eight different LDA and GGA functionals, the performances for computing the geometries and relative energies of the stationary points along the PES of our model reaction (see Chart 1) were compared. These density functionals are the LDA functional VWN³⁶ and the GGA functionals BP86,^{37,38} BLYP,^{37,39} PW91,^{40–43} PBE,^{44,45} revPBE,⁴⁶ RPBE,⁴⁷ and OLYP.^{39,48} They were used in combination with the TZ2P basis set, which is a large uncontracted set of Slater-type orbitals (STOs) containing diffuse functions, which is of triple- ζ quality and has been augmented with two sets of polarization functions: 2p and 3d on H, 3d and 4f on C and Cl, 5p and 4f on Pd. The core shells of carbon (1s), chlorine (1s2s2p), and palladium (1s2s2p3s3p3d) were treated by the frozen-core approximation.³² An auxiliary set of s, p, d, f, and g STOs was used to fit the molecular density and to represent the Coulomb and exchange potentials accurately in each SCF cycle.³² Relativistic effects were accounted for using the zeroth-order regular approximation (ZORA).⁴⁹ For each of the eight functionals, all stationary points were confirmed to be equilibrium structures (no imaginary frequencies) or a

Table 1. Basis Sets Used in the *ab Initio* Calculations

name	Pd	C	H	Cl
BS1	(24s16p13d) ^a	cc-aug-pVDZ ^b	cc-aug-pVDZ ^b	cc-aug-pVTZ ^b
BS2	(24s16p13d) ^a + 1f	cc-aug-pVDZ ^b	cc-aug-pVDZ ^b	cc-aug-pVTZ ^b
BS2(−)	(24s16p13d) ^a + 1f	cc-aug-pVDZ ^b	cc-aug-pVDZ ^b	cc-aug-pVDZ ^b
BS2(+)	(24s16p13d) ^a + 1f	cc-aug-pVTZ ^b	cc-aug-pVTZ ^b	cc-aug-pVTZ ^b
BS3	(24s16p13d) ^a + 4f	cc-aug-pVDZ ^b	cc-aug-pVDZ ^b	cc-aug-pVTZ ^b
BS4	(24s16p13d) ^a + 4f + p	cc-aug-pVDZ ^b	cc-aug-pVDZ ^b	cc-aug-pVTZ ^b
BS5	(24s16p13d) ^a + 4f + p + g	cc-aug-pVDZ ^b	cc-aug-pVDZ ^b	cc-aug-pVTZ ^b

^a TZP quality. ^b Completely uncontracted.

transition state (one imaginary frequency) through vibrational analysis. Enthalpies at 298.15 K and 1 atm were calculated from 0 K electronic energies according to the following equation, assuming an ideal gas:

$$\Delta H_{298} = \Delta E + \Delta E_{\text{trans},298} + \Delta E_{\text{rot},298} + \Delta E_{\text{vib},0} + \Delta(\Delta E_{\text{vib},0})_{298} + \Delta(pV)$$

Here, $\Delta E_{\text{trans},298}$, $\Delta E_{\text{rot},298}$, and $\Delta E_{\text{vib},0}$ are the differences between products and reactants in translational, rotational, and zero-point vibrational energies, respectively; $\Delta(\Delta E_{\text{vib},0})_{298}$ is the change in the vibrational energy difference going from 0 to 298.15 K. The vibrational energy corrections are based on our frequency calculations. The molar work term $\Delta(pV)$ is $(\Delta n)RT$; $\Delta n = -1$ for two reactants (Pd + CH₃Cl) combining to one species. Thermal corrections for the electronic energy are neglected.

2.2. *Ab Initio* Calculations. On the basis of the ZORA-BLYP/TZ2P geometries, energies of the stationary points were computed in a series of single-point calculations with the program package DIRAC^{50,51} using the following hierarchy of quantum chemical methods: HF, MP2, CCSD, and CCSD(T). Relativistic effects are accounted for using a full all-electron four-component Dirac–Coulomb approach with a spin-free Hamiltonian.⁵² The two-electron integrals exclusively over the small components have been neglected and corrected with a simple Coulombic correction, which has been shown to be reliable.⁵³

A hierarchical series of Gaussian-type basis sets was used (see Table 1). For carbon, hydrogen, and chlorine, Dunning's correlation consistent augmented double- ζ (cc-aug-pVDZ) and triple- ζ (cc-aug-pVTZ) basis sets were used.^{54,55} These were used in uncontracted form because it is technically difficult to use contracted basis sets in the kinetic balance procedure in DIRAC.⁵⁶ The basis set of palladium is based on an uncontracted basis set (24s16p13d), which is of triple- ζ quality, and has been developed by K. Faegri, Jr. (personal communication). The combination of this basis set for palladium and the aforementioned cc-aug-pVDZ basis set for carbon and hydrogen and cc-aug-pVTZ basis set for chlorine is denoted BS1 (see Table 1). As a first extension, in BS2, one set of 4f polarization functions was added with an exponent of 1.472, as reported by Ehlers et al.⁵⁷ In BS3, this single set of 4f functions was substituted by four sets of 4f polarization functions as reported by Langhoff and co-workers with exponents of 3.611 217, 1.295 41, 0.554 71, and 0.237 53.⁵⁸ Thereafter, going to BS4, an additional set of diffuse p functions was introduced with an exponent of 0.141 196, as proposed by Osanai et al.⁵⁹ BS5 was created

by adding a set of g functions, with an exponent of 1.031 690 071. This value is close but not exactly equal to the exponent of the g functions optimized by Osanai. Instead, it is equal to the value of one of the exponents of the d set of Faegri, which reduces computational costs.

Note that the basis sets BS1–BS5 used in the present study (see Table 1) correspond in quality to the basis sets BS1–BS5 used in our recent studies on the oxidative addition of Pd to the C–C bond of ethane and the C–F bond of fluoromethane (see Table 2 in ref 27 and Table 1 in ref 28, respectively), using, however, an uncontracted cc-aug-pVTZ basis set for chlorine. For the C–C addition reaction, concerning the uncontracted cc-aug-pVDZ basis set for C and H, relative energies were converged to within ca. 1 kcal/mol at BS5. For the present reaction, we have investigated more extensively how well the relative energies are converged with respect to the basis-set sizes of carbon, hydrogen, and chlorine. To this end, basis sets BS2(−) and BS2(+) were also constructed. BS2(−) is equal to BS2, but with a cc-aug-pVDZ instead of a cc-aug-pVTZ basis set for chlorine. BS2(+) also corresponds to BS2, but with a cc-aug-pVTZ basis set for all three elements C, H, and Cl. For a schematic overview, see Table 1.

2.3. DFT Calculations. On the basis of the ZORA-BLYP/TZ2P geometries, we have also evaluated, in a series of single-point calculations, how the ZORA-BLYP relative energies of stationary points along the PES depend on the basis-set size for four different all-electron (i.e., no frozen-core approximation) STO basis sets, namely, ae-DZ, ae-TZP, ae-TZ2P, and ae-QZ4P, and on the use of the frozen-core approximation. The ae-DZ basis set is of double- ζ quality and is unpolarized for C, Cl, and H but has been augmented with a set of 5p polarization functions for Pd. The ae-TZP basis set is of triple- ζ quality and has been augmented with one set of polarization functions on every atom: 2p on H, 3d on C and Cl, and 5p on Pd. The ae-TZ2P basis set (the all-electron counterpart corresponding to the above-mentioned TZ2P basis that is used in conjunction with the frozen-core approximation) is also of triple- ζ quality and has been augmented with two sets of polarization functions on each atom: 2p and 3d on H, 3d and 4f on C and Cl, and 5p and 4f on Pd. The ae-QZ4P basis set is of quadruple- ζ quality and has been augmented with four sets of polarization functions on each atom (five for chlorine): two 2p and two 3d sets on H, two 3d and two 4f sets on C, three 3d and two 4f sets on Cl, and two 5p and two 4f sets on Pd.

Finally, again on the basis of the ZORA-BLYP/TZ2P geometries, we have computed, in a post-self-consistent-field

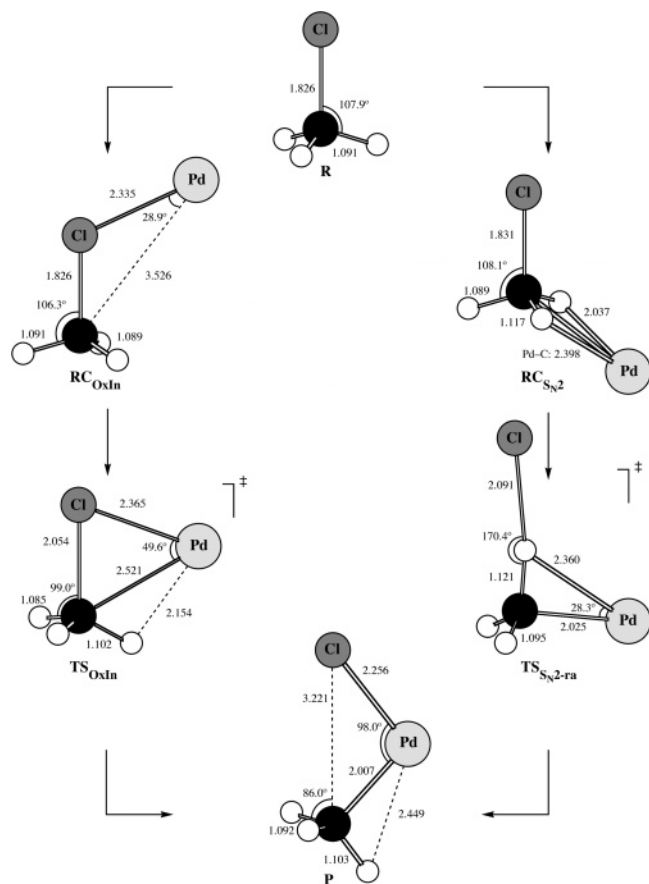


Figure 1. Structures of stationary points along the reaction coordinates of the OxIn- and S_N2-type pathways for oxidative addition of the C–Cl bond of CH₃Cl to Pd. Geometry optimized at ZORA-BLYP/TZ2P, i.e., with frozen-core approximation.

(post-SCF) manner, that is, using in all cases the electron density obtained at ZORA-BLYP/ae-TZ2P, the relative energies of stationary points along the PES for various LDA, GGA, meta-GGA, and hybrid functionals. In addition to the ones used in the geometry optimizations (see Section 2.1), the following density functionals were examined: the GGA functionals Becke 88x + BR89c,^{60,61} FT97,⁶² HCTH/93,⁶³ BOP,^{60,64} HCTH/120,⁶⁵ HCTH/147,⁶⁵ and HCTH/407,⁶⁶ the meta-GGA functionals BLAP3,⁶⁷ VS98,⁶⁸ KCIS,⁶⁹ PKZB,^{70,71} Bmτ1,⁷² OLAP3,^{48,67} and TPSS,^{73,74} and the hybrid functionals B3LYP,^{75,76} O3LYP,⁷⁷ X3LYP⁷⁸ (all based on VWN5⁷⁹), and TPSSh.^{73,74}

3. Results and Discussion

3.1. Geometries of Stationary Points and Characteristics of the Addition Reaction. First, we examine the geometries of stationary points along the reaction coordinates of the two pathways for the oxidative addition of Pd to the C–Cl bond of chloromethane, computed with the LDA functional VWN and the GGA functionals BP86, BLYP, PW91, PBE, revPBE, RPBE, and OLYP in combination with the TZ2P basis set, the frozen-core approximation, and the ZORA to account for relativistic effects. For the BLYP functional, the results are given in Figure 1. For the other functionals, the optimized geometries are given in the Supporting Information, in Figure S1 and Table S1.

For each of the functionals, the reaction characteristics are similar. For the direct insertion (OxIn) pathway, the reaction proceeds from the reactants R via the formation of a stable, C_s symmetric reactant complex, RC_{OxIn}, in which the chlorine atom coordinates to Pd, to a transition state, TS_{OxIn}, of C_s symmetry and, finally, a stable product P of C_s symmetry (see Figure 1). For the alternative S_N2 pathway, the reaction proceeds from the reactants via formation of another stable, C_s symmetric reactant complex, RC_{SN2}, in which chloromethane coordinates via two hydrogen atoms in an η² fashion to Pd (see Figure 1), completely analogous to reactant complexes for the reaction of Pd with methane,²⁶ ethane,²⁷ and fluoromethane.²⁸ From RC_{SN2}, the S_N2 substitution then occurs in concert with a rearrangement of the Cl[−] leaving group from carbon to palladium, with a transition state TS_{SN2-ra} of C_s symmetry and, finally, the same product P as in the OxIn pathway.

We wish to point out the two marked differences between the S_N2-ra mechanism of the Pd + CH₃Cl system tackled in the present investigation (see also refs 3 and 10) and that of Pd + CH₃F, studied recently.²⁸ In both cases, there are two competing reaction channels, direct oxidative insertion (OxIn) and an alternative pathway with strong S_N2 character (S_N2-ra). In the first place, however, the C–F bond is much stronger than the C–Cl bond, and activation of the former is associated with significantly higher barriers (via both OxIn and S_N2). Thus, at variance with the situation for Pd + CH₃Cl, the minimum energy path for Pd approaching CH₃F from the backside is, in a sense, redirected from straight nucleophilic substitution and proceeds instead via the relatively low-energy saddle point TS_{CH} for insertion into a C–H bond. Furthermore, for both, Pd + CH₃F and Pd + CH₃Cl, the highest point on the PES of the S_N2-ra pathway has the character of a migrating leaving group, that is, F[−] and Cl[−], respectively, that is expelled during the actual substitution process. However, the much higher basicity of F[−] compared to Cl[−] causes the former, after its expulsion in the actual S_N2 transition state TS_{SN2} and on its way toward Pd, to abstract a proton, under formation of the intermediate complex IM_{SN2} between PdCH₂ and HF (see ref 28). From the latter, fluoride migrates via transition state TS_{SN2-ra} toward Pd under formation of the product CH₃PdF. At variance, in the case of Pd + CH₃Cl, the expelled Cl[−] leaving group migrates directly to Pd *without abstracting a proton* and, thus, without forming an additional intermediate complex involving the conjugate acid HCl. Thus, the only transition state encountered along the reaction coordinate of the nucleophilic substitution reaction between Pd and CH₃Cl is the one with chloride rearrangement character: TS_{SN2-ra}.

All species in both reaction pathways have been verified through vibrational analyses to represent equilibrium structures (no imaginary frequencies) or transition states (one imaginary frequency). Furthermore, it has been verified that each transition state connects the stable stationary points as reported.

The geometries obtained with the various LDA and GGA functionals do not show significant mutual discrepancies (see Table S1 and Figure S1 in the Supporting Information). One

Table 2. Relative Energies (in kcal/mol) of the Stationary Points along the Reaction Coordinates of the OxIn- and S_N2-type Pathways for Oxidative Addition of the C–Cl Bond of CH₃Cl to Pd, without (no CPC) and with Counterpoise Correction (with CPC), Computed at Several Levels of ab Initio Theory

method	basis set	RC _{OxIn}		RC _{S_N2}		TS _{OxIn}		TS _{S_N2-ra} ^a		P	
		no CPC	with CPC	no CPC	with CPC	no CPC	with CPC	no CPC	with CPC	no CPC	with CPC
HF	BS1	6.4	6.9	9.9	10.4	28.9	29.4	61.6	62.2	4.3	4.8
	BS2	6.2	6.7	9.8	10.3	28.6	29.2	60.6	61.1	2.0	2.6
	BS2(–)	7.2	7.7	9.8	10.3	29.0	29.6	58.6	59.1	1.6	2.2
	BS2(+)	6.2	6.7			28.4	28.9				
	BS3	6.0	6.5	9.5	10.1	28.2	28.8	59.6	60.2	0.1	0.8
	BS4	6.0	6.5	9.6	10.0	28.2	28.7	59.6	60.1	0.0	0.6
	BS5	5.9	6.4	9.5	10.0	28.1	28.6	59.3	59.9	–0.6	0.0
MP2	BS1	–11.2	–6.4	–5.8	–0.9	3.9	10.4	41.9	47.3	–29.5	–19.7
	BS2	–16.7	–9.8	–10.6	–3.5	–3.1	6.2	37.3	45.1	–39.0	–25.0
	BS2(–)	–10.8	–6.2	–10.1	–3.3	1.7	9.3	36.7	44.4	–34.3	–22.6
	BS2(+)	–17.4	–10.0			–8.5	4.6				
	BS3	–16.9	–13.7	–9.6	–6.5	–2.0	1.8	45.1	48.6	–30.4	–25.0
	BS4	–16.3	–14.2	–7.7	–6.0	–1.1	1.4	46.4	48.6	–29.4	–25.4
	BS5	–16.7	–14.8	–9.0	–7.3	–1.8	0.5	46.7	48.7	–29.1	–25.4
CCSD	BS1	–8.3	–3.5	–4.3	0.7	7.2	13.6	40.0	45.5	–28.7	–19.1
	BS2	–11.3	–5.3	–6.9	–0.7	3.6	11.8	38.2	45.1	–33.8	–21.8
	BS2(–)	–6.5	–2.2	–6.6	–0.5	7.4	14.2	37.4	44.3	–29.9	–19.7
	BS2(+)	–11.9	–5.4			–0.8	10.4				
	BS3	–10.2	–7.3	–5.0	–2.3	6.4	9.7	44.9	48.1	–27.1	–22.4
	BS4	–9.8	–7.8	–4.1	–2.6	7.0	9.3	45.9	48.0	–26.4	–22.8
	BS5	–9.6	–7.9	–4.2	–2.8	6.9	9.1	46.4	48.4	–25.8	–22.5
CCSD(T)	BS1	–11.0	–5.1	–7.0	–0.8	2.1	10.0	35.0	42.0	–33.8	–22.3
	BS2	–14.9	–7.7	–10.3	–2.7	–2.6	7.1	31.7	40.2	–40.7	–26.5
	BS2(–)	–9.4	–4.2	–9.9	–2.5	1.9	10.1	31.1	39.5	–36.1	–24.0
	BS2(+)	–15.6	–7.9			–7.7	5.5				
	BS3	–14.1	–10.3	–8.5	–4.7	0.2	4.7	38.5	43.1	–33.6	–27.6
	BS4	–13.1	–11.0	–6.8	–5.0	1.6	4.2	40.3	43.0	–32.0	–28.0
	BS5	–13.1	–11.2	–7.0	–5.4	1.4	3.8	40.7	43.3	–31.7	–28.0

^a CCSD(T) procedure not reliable for C–Cl S_N2 transition state, see Section 3.2.

eye-catching, but not essential, difference is the product P computed with VWN and PW91. Here, the methyl group is rotated into an eclipsed instead of a staggered conformation relative to the Pd–Cl bond, at variance with the product geometries for the other functionals. It should be noted, however, that enforcing a staggered geometry will raise the energy by only 0.2 kcal/mol for VWN and a virtually negligible 0.03 kcal/mol for PW91. In fact, the essential physics here is that the methyl group is virtually a free internal rotor.

The C–H bond distance values are very robust with respect to changing the functional, with variations on the order of a few hundredths, or less, of an angstrom. Note that variations in the length of the activated C–Cl bond become larger, up to ca. 0.2 Å in the product, as the reaction progresses. This is in line with the fact that this bond is being broken along the reaction coordinate, which causes the PES to become increasingly soft in this coordinate and, thus, sensitive to changes in the computational method. More pronounced variations are found for the weak Pd–C, Pd–H, and Pd–Cl bonds. This holds especially for the loosely bound reactant complex RC_{S_N2} and the unstable transition state TS_{S_N2-ra}, which for the GGA functionals show fluctuations of up to more than 0.1 Å for Pd–C and Pd–Cl (LDA deviates a bit more, up to 0.5 Å for Pd–Cl). The

variations in these bond distances drop to a few hundredths or even a few thousandths of an angstrom as the reaction proceeds to the product in which more stable coordination bonds are formed.

Thus, the various functionals yield essentially the same geometries. Because we found in previous studies on the reaction of Pd with methane and ethane that BLYP performed excellently in terms of the relative energies of stationary points for those model reactions^{26,27} and because BLYP is robust and well established, we chose the geometries of this functional, that is, ZORA-BLYP/TZ2P, to compute the ab initio benchmark potential energy surface in the next section.

3.2. Benchmark Energies from ab Initio Calculations.

Here, we report the first systematic ab initio calculations into relative energies of the model addition reaction of the C–Cl bond of chloromethane to the Pd atom. This survey is based on geometries of stationary points that were optimized at the ZORA-BLYP/TZ2P level of relativistic DFT (see preceding section and Figure 1). The results of our ab initio computations are collected in Tables 2 and 3 (relative energies and BSSE). Tables S2 and S3 in the Supporting Information show the total energies in atomic units of all species occurring at the stationary points as well as the BSSE for all methods and all stationary points. The reaction profiles

Table 3. Basis Set Superposition Error (BSSE, in kcal/mol) for Pd and CH₃Cl in the Stationary Points along the Reaction Coordinates of the OxIn- and S_N2-type Pathways for Oxidative Addition of the C–Cl Bond of CH₃Cl to Pd, Computed at the CCSD(T) Level of ab Initio Theory

basis set	RC _{OxIn}			RC _{S_N2}			TS _{OxIn}			TS _{S_N2-ra}			P		
	Pd	CH ₃ Cl	total	Pd	CH ₃ Cl	total	Pd	CH ₃ Cl	total	Pd	CH ₃ Cl	total	Pd	CH ₃ Cl	total
BS1	5.5	0.4	5.9	5.9	0.3	6.2	7.4	0.5	7.9	6.2	0.7	6.9	10.6	0.9	11.5
BS2	6.8	0.4	7.2	7.2	0.3	7.5	9.2	0.5	9.7	7.8	0.7	8.5	13.2	1.0	14.1
BS2(–)	4.3	0.8	5.1	6.9	0.5	7.4	7.2	1.0	8.2	7.7	0.8	8.5	10.4	1.7	12.1
BS2(+)	7.4	0.3	7.7				12.9	0.3	13.2						
BS3	3.2	0.7	3.8	3.2	0.5	3.7	3.6	0.9	4.5	3.5	1.1	4.6	4.5	1.6	6.1
BS4	1.4	0.8	2.2	1.2	0.6	1.8	1.6	1.0	2.6	1.4	1.3	2.7	2.3	1.7	4.1
BS5	1.1	0.8	1.9	1.1	0.6	1.7	1.3	1.1	2.4	1.2	1.4	2.6	1.8	1.8	3.7

obtained with CCSD(T) are graphically displayed in Figure S2 in the Supporting Information.

We proceed with examining the reaction profiles of the two pathways for the oxidative addition of Pd to the chloromethane C–Cl bond, that is, the energies of the stationary points relative to the reactants Pd and chloromethane (see Table 2 and Figure S2, Supporting Information). At almost all levels of theory except Hartree–Fock, the reaction profiles are characterized by the formation of stable reactant complexes RC_{OxIn} and RC_{S_N2}, where the first one is always lower in energy than the second one, which lead via the transition state for direct oxidative insertion (TS_{OxIn}) or via the transition state for rearrangement after the S_N2 reaction (TS_{S_N2-ra}) to the oxidative addition product (P). Three striking observations can be made: (i) the spread in values of computed relative energies, depending on the level of theory and basis set, is enormous, up to ca. 45 kcal/mol; (ii) the size of the BSSE is also remarkably large, up to ca. 14 kcal/mol; (iii) without counterpoise correction, convergence with basis-set size of the computed energies is still not reached with standard basis sets used routinely in CCSD(T) computations on organometallic and coordination compounds. The lack of any correlation, which is important for this model reaction,^{80,81} leads to a complete failure at the HF level, which yields unbound reactant complexes and strongly exaggerated activation barriers: ca. 29 kcal/mol for TS_{OxIn} and ca. 60 kcal/mol for TS_{S_N2-ra}. The activation energies for both pathways drop significantly when electron correlation is introduced. Along HF, CCSD, and CCSD(T) in combination with basis set BS1, for example, the activation barrier for direct oxidative insertion decreases from 28.9 to 7.2 to 2.1 kcal/mol (see Table 2). But also, the correlated CCSD(T) values obtained with basis sets BS1 up to BS3, comparable in quality to standard basis sets such as LANL2DZ^{82,83} without or with up to four *f* functions added, are questionable, if one does not take into account counterpoise correction, as they are obviously not converged as a function of the basis-set size. For example, at CCSD(T)/BS1, the activation energy for direct insertion is 2.1 kcal/mol. This activation energy computed at CCSD(T) drops from 2.1 kcal/mol for basis set BS1 to –2.6 kcal/mol for basis set BS2 in which one *f* polarization function has been added. Thereafter, along BS2 to BS5, the activation energy increases again, although not monotonically, from –2.6 to 1.4 kcal/mol, as three more sets of *f* functions, an

additional set of diffuse *p* functions, and a set of *g* functions are added to the basis set of Pd (see Tables 1 and 2).

Next, we note that the BSSE takes on large values in the correlated ab initio methods. At the CCSD(T) level, for example, the BSSE for TS_{OxIn} amounts to 7.9, 9.7, 4.5, 2.6, and 2.4 kcal/mol along the basis sets BS1–BS5 (Table 3), whereas the corresponding BSSE values at HF are only ca. 0.6 kcal/mol. The BSSE increases along the reaction coordinate, that is, going from RC_{OxIn} to TS_{OxIn} to P, or going from RC_{S_N2} to TS_{S_N2-ra} to P. The reason for this is that, along these series of stationary points, the carbon, hydrogen, and chlorine atoms and, thus, their basis functions come closer and begin to surround the palladium atom. This effectively improves the flexibility and polarization of the basis set and, thus, the description of the wave function in the region of the palladium atom. Note that the BSSE stems predominantly from the improvement of the stabilization of palladium as chloromethane ghost functions are added. This contribution to the BSSE quickly reduces as the basis set of palladium is improved, and for the two largest basis sets, BS4 and BS5 (which contain *g* as well as diffuse *p* functions on Pd), it is on the same order as the extra stabilization of the chloromethane fragment due to adding palladium ghost functions. Note that the total BSSE at CCSD(T) has been considerably decreased, that is, from 9.7 kcal/mol for BS2 to only 2.4 kcal/mol for BS5 (Table 3), and is, thus, not much larger anymore than the relative energies that we compute, in particular, the OxIn barrier of 1.4 kcal/mol, see CCSD(T)/BS5 in Table 2.

In basis sets BS1, BS2, BS3, BS4, and BS5, mentioned above, we use consistently the same basis sets for all substrate atoms, namely, the uncontracted cc-aug-pVDZ for carbon and hydrogen and cc-aug-pVTZ for chlorine. For the oxidative addition of the methane C–H bond to Pd, it was shown that counterpoise-corrected CCSD(T) relative energies at BS5, that is, using uncontracted cc-aug-pVDZ for C and H, are converged within ca. 1 kcal/mol with respect to extending the basis set for C and H to uncontracted cc-aug-pVTZ.²⁷ Here, we explore to what extent counterpoise-corrected CCSD(T) relative energies of the Pd + CH₃Cl system are converged if the basis set for C and H is extended from cc-aug-pVDZ in basis set BS2 to cc-aug-pVTZ in the larger basis set BS2(+) (see Table 1). Furthermore, we probe the dependence of the counterpoise-corrected CCSD(T) relative energies on the size of the basis set for Cl by

reducing it from cc-aug-pVTZ in basis set BS2 to cc-aug-pVDZ in basis set BS2(−) (see Table 1). The results for the modified basis sets BS2(−) and BS2(+) are also shown in Tables 2 and 3 below the entry for basis set BS2. It appears that using cc-aug-pVDZ instead of cc-aug-pVTZ for chlorine makes a significant difference for the counterpoise-corrected CCSD(T) relative energies. The barrier for oxidative insertion (TS_{OxIn}), for example, changes from 7.1 to 10.1 kcal/mol, going from BS2 to BS2(−) [see Table 2, CCSD(T) with CPC]. From this, we conclude that using the uncontracted cc-aug-pVTZ basis set for the chlorine in chloromethane is a minimal requirement. The calculations with basis set BS2(+) are extremely expensive and were, therefore, confined to the relative energies of two stationary points: RC_{OxIn} and TS_{OxIn} . In agreement with our earlier finding for $Pd + CH_4$,²⁷ extending the basis sets of C and H from cc-aug-pVDZ to cc-aug-pVTZ has little effect on the counterpoise-corrected CCSD(T) relative energies. The barrier for oxidative insertion (TS_{OxIn}), for example, decreases by only 1.5 kcal/mol, from 7.1 to 5.5 kcal/mol, going from BS2 to BS2(+) (see Table 2, CCSD(T) with CPC). We conclude that using uncontracted cc-aug-pVDZ for C and H and uncontracted cc-aug-pVTZ for Cl represents a good compromise between computational efficiency and accuracy in our CCSD(T) computations.

Thus, we have been able to achieve virtual convergence of the CCSD(T) relative energies by using a larger than standard basis set and by correcting for the BSSE through counterpoise correction, see Table 2. The counterpoise-corrected relative energies at CCSD(T) are converged to within some tenths of a kilocalorie per mole. For example, the counterpoise-corrected activation energy for direct oxidative insertion (OxIn) at CCSD(T) amounts to 10.0, 7.1, 4.7, 4.2, and 3.8 kcal/mol.

There are, however, strong indications for one of the species, the transition state of the S_N2 pathway TS_{S_N2-ra} , being problematic in the sense that a single-reference ab initio approach to describing it [e.g., HF, MP2, or CCSD(T)] is not suitable: (i) unlike the situation for the other species, the HOMO and LUMO of TS_{S_N2-ra} are degenerate within a few hundredths of an electronvolt; (ii) in line with this, there is near degeneracy of the singlet and triplet states [$E_{triplet} - E_{singlet} = +1.3, -11.0, +3.7, -5.8$, and -1.6 kcal/mol at BLYP/TZ2P, HF, MP2, CCSD, and CCSD(T); ab initio values obtained with BS5 and CPC], and (iii) importantly, the resulting activation energy of 43.3 kcal/mol at CCSD(T)/BS5 with CPC is also much higher than all barriers obtained with the various density functionals, even those which normally overestimate this type of reaction barrier, such as OLYP. For example, the activation barriers obtained with BLYP, OLYP, and B3LYP are 23.1, 31.9, and 36.3 kcal/mol, respectively, all well below the CCSD(T) value of 43.3 kcal/mol. An analysis of the electronic structure of TS_{S_N2-ra} reveals the physics behind this phenomenon: the species has much of the character of a complex between Cl^- and $PdCH_3^+$. Consequently, the HOMO and LUMO of TS_{S_N2-ra} closely resemble a chlorine 3p atomic orbital (AO), pushed up in energy by the (local) excess of negative charge, and a carbon 2p AO on the methyl fragment in $PdCH_3^+$,

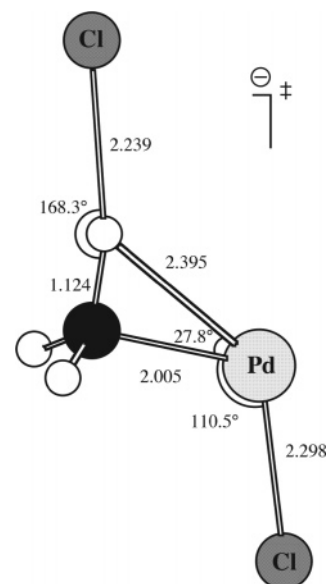


Figure 2. Structure of the S_N2-ra transition state for oxidative addition of the C–Cl bond of CH_3Cl to $PdCl^-$. Geometry optimized at ZORA-BLYP/TZ2P, i.e., with frozen-core approximation.

pulled down in energy by the (local) excess of positive charge: these circumstances clearly promote the occurrence of a single-electron transfer from Cl^- to $PdCH_3^+$. This suggests that the problem may be relieved if the LUMO is destabilized. This can be achieved, for example, by introducing an extra chloride ligand at palladium, which neutralizes the excess positive charge in the $PdCH_3^+$ moiety of TS_{S_N2-ra} . Thus, we have computed and analyzed the corresponding transition state for $PdCl^-$ (instead of Pd) induced C–Cl bond activation, the structure of which is shown in Figure 2. Indeed, all indicators of a pathological situation disappear: (i) there is a clear HOMO–LUMO gap of 0.65 eV at BLYP/TZ2P; (ii) the singlet state is well below the triplet state, and (iii) the counterpoise-corrected CCSD(T)/BS3⁸⁴ value for the energy relative to the reactants again agrees perfectly with the BLYP/TZ2P value—both amount to -18.8 kcal/mol (not shown in a Table).⁸⁵

In conclusion, our best estimate, obtained at CCSD(T)/BS5 with CPC, for the kinetic and thermodynamic parameters of the oxidative insertion of Pd into the chloromethane C–Cl bond is -11.2 kcal/mol for the formation of the reactant complex leading to the direct oxidative insertion (OxIn) pathway, -5.4 kcal/mol for the formation of the reactant complex leading to the S_N2 pathway, 3.8 kcal/mol for the activation energy (relative to the reactants) for the OxIn pathway, and -28.0 kcal/mol for the reaction energy (see Table 4). The activation energy of 43.3 kcal/mol for the S_N2 pathway is probably too high for the reasons pointed out above; this value should, therefore, be treated with great precaution and not as a benchmark. If we take into account zero-point vibrational energy (ZPE) effects computed at BLYP/TZ2P, we arrive at -10.8 kcal/mol for the formation of the reactant complex leading to the OxIn pathway, -6.1 kcal/mol for the formation of the reactant complex leading to the S_N2 pathway, 2.7 kcal/mol for the activation energy

Table 4. Relative Energies without (ΔE) and with Zero-Point Vibrational Energy Correction ($\Delta E + \Delta ZPE$) and Relative Enthalpies at 298.15 K (ΔH) of the Stationary Points^a along the Reaction Coordinates of the OxIn- and S_N2-type Pathways for Oxidative Addition of the C–Cl Bond of CH₃Cl to Pd (in kcal/mol), Computed with Eight Different Density Functionals and the TZ2P Basis Set with Frozen-Core Approximation,^b and Compared to the ab Initio Benchmark from This Work

method	ΔE					$\Delta E + \Delta ZPE$					ΔH				
	RC _{OxIn}	RC _{S_N2}	TS _{OxIn}	TS _{S_N2-ra}	P	RC _{OxIn}	RC _{S_N2}	TS _{OxIn}	TS _{S_N2-ra}	P	RC _{OxIn}	RC _{S_N2}	TS _{OxIn}	TS _{S_N2-ra}	P
DFT Computations (This Work) ^b															
VWN	–30.1	–25.5	–21.8	15.8	–52.1	–29.6	–26.6	–22.7	11.8	–52.9	–29.9	–27.1	–23.2	11.4	–53.1
BP86	–16.4	–9.3	–5.2	23.4	–36.9	–16.0	–10.2	–6.3	20.4	–37.7	–16.2	–10.6	–6.8	20.1	–37.8
BLYP	–12.9	–5.1	–0.6	23.1	–33.1	–12.5	–5.8	–1.7	20.4	–33.9	–12.7	–6.0	–2.0	20.1	–34.0
PW91	–17.6	–10.8	–6.7	22.7	–37.8	–17.1	–11.6	–7.8	19.8	–38.7	–19.1	–12.0	–10.0	19.5	–39.4
PBE	–17.0	–10.4	–6.1	23.3	–37.1	–16.6	–11.3	–7.2	20.3	–37.9	–16.8	–11.7	–7.7	19.9	–38.7
revPBE	–11.9	–5.0	0.1	26.1	–31.4	–11.6	–5.9	–1.0	23.5	–32.3	–11.8	–6.1	–1.4	23.1	–32.4
RPBE	–11.5	–4.5	0.8	26.1	–30.7	–11.1	–5.3	–0.4	23.3	–31.5	–11.3	–5.6	–0.7	23.0	–31.7
OLYP	–6.8	–0.1	7.0	31.2	–23.5	–6.4	–0.8	5.8	28.7	–24.4	–6.6	–0.9	5.3	28.4	–24.5
Ab Initio Benchmark (This Work) ^c															
CCSD(T)	–11.2	–5.4	3.8	(43.3) ^d	–28.0	–10.8	–6.1	2.7	(40.6) ^d	–28.8					

^a Geometries and energies computed at the same level of theory. See Figure S1 and Table S1 in the Supporting Information for structures.

^b Relativistic effects treated with ZORA (see Section 2). ^c CCSD(T) benchmark from this work, based on BLYP-optimized geometries. ^d CCSD(T) procedure not reliable for C–Cl S_N2 transition state, see Section 3.2.

(relative to the reactants) for the OxIn pathway, and –28.8 kcal/mol for the reaction energy (see Table 4).

3.3. Validation of DFT. Next, we examine the relative energies of stationary points computed with the LDA functional VWN and the GGA functionals BP86, BLYP, PW91, PBE, revPBE, RPBE, and OLYP in combination with the TZ2P basis set, the frozen-core approximation, and the ZORA to account for relativistic effects. Note that for each density functional we consistently use the geometries optimized with that functional, for example, BP86//BP86 or BLYP//BLYP (see Section 3.1). We focus on the overall activation energy, that is, the difference in energy between the transition state and the separate reactants, which is decisive for the rate of chemical reactions in the gas phase, in particular, if they occur under low-pressure conditions in which the reaction system is (in good approximation) thermally isolated^{86,87} (see also Section 2 of ref 88). Relative energies, with and without zero-point vibrational energy correction, as well as relative enthalpies are collected in Table 4 and graphically represented in Figure S3 in the Supporting Information. The performance of the LDA functional VWN and the seven different GGA functionals is assessed by a systematic comparison of the resulting potential energy surfaces with our relativistic four-component CCSD(T) benchmark. It is clear from Table 4 that LDA suffers here from its infamous overbinding, providing barriers that are too low and complexation and reaction energies that are too high. The GGA functionals fall into three groups regarding their agreement with the benchmark results. OLYP clearly underestimates metal–substrate bonding and yields too weakly bound reactant complexes for both pathways, a barrier for the OxIn pathway that is too high by 3.2 kcal/mol, and an insufficiently exothermic reaction energy. The situation is the opposite for BP86, PBE, and PW91, which overestimate metal–substrate bonding, giving rise to too strongly bound reactant complexes, a significantly underestimated barrier for the OxIn pathway (by more than 10 kcal/mol for PW91), and a too exothermic reaction energy. On the other hand, BLYP and the two revisions of

PBE, that is, revPBE and RPBE, perform very satisfactorily with reactant complexes in good agreement with the coupled-cluster PES and a relatively small underestimation of the barrier for the OxIn pathway (i.e., by 4.4, 3.7, and 3.0 kcal/mol for BLYP, revPBE, and RPBE, respectively) and somewhat too large reaction energies, but less so than in the case of the group of BP86, PBE, and PW91. Note that all density functionals undershoot to an unusually high extent the CCSD(T) value of the barrier associated with the S_N2 pathway. In Section 3.2, it was pointed out that in this case (i.e., for TS_{S_N2-ra}) the CCSD(T) value tends to be too high and should be treated with great precaution (later on, the issue is again briefly addressed).

We proceed with examining the convergence of the (all-electron) BLYP relative energies of stationary points as the basis set increases along ae-DZ, ae-TZP, ae-TZ2P, and ae-QZ4P, using the ZORA-BLYP/TZ2P geometries, which were also used in the ab initio calculations in the preceding section (see Figure 1). We also investigate the convergence of the BSSE along this series and the effect of using the frozen-core approximation in the calculations discussed in the preceding paragraph. The results are shown in Table 5 and in Figure S4 in the Supporting Information. In the first place, we note that it is valid to use the frozen-core approximation as it has only small effects on the relative energies. This becomes clear if one compares, in Table 5, the frozen-core BLYP/TZ2P results (no CPC: –12.9, –5.1, –0.6, 23.1, and –33.1 kcal/mol for RC_{OxIn}, RC_{S_N2}, TS_{OxIn}, TS_{S_N2-ra}, and P, respectively) with the corresponding all-electron BLYP/ae-TZ2P data (no CPC: –12.8, –5.1, –0.5, 23.1, and –33.5 kcal/mol for RC_{OxIn}, RC_{S_N2}, TS_{OxIn}, TS_{S_N2-ra}, and P, respectively). The frozen-core and all-electron values of the relative energies agree within 0.1–0.4 kcal/mol. Likewise, the BSSE values computed with the frozen-core TZ2P and ae-TZ2P basis sets agree within 0.1 kcal/mol (see Table 5). Next, the issue of basis set convergence is addressed. The data in Table 5 show that the relative energies of stationary points are already converged to within the order of some tenths of a kilocalorie per mole with the ae-TZ2P

Table 5. Relative Energies (in kcal/mol) of the Stationary Points^a along the Reaction Coordinates of the OxIn- and S_N2-type Pathways for Oxidative Addition of the C–Cl Bond of CH₃Cl to Pd, Computed with BLYP and Four Different Basis Sets with All Electrons Treated Variationally, without (no CPC) and with Counterpoise Correction (with CPC)^b

basis set	RC _{OxIn}		RC _{S_N2}		TS _{OxIn}		TS _{S_N2-ra}		P	
	no CPC	with CPC	no CPC	with CPC	no CPC	with CPC	no CPC	with CPC	no CPC	with CPC
ae-DZ	−6.5	−4.4	−2.4	0.5	1.9	5.3	16.8	19.0	−32.8	−29.6
ae-TZP	−12.0	−11.9	−4.6	−4.4	0.3	0.5	23.0	23.4	−31.8	−31.4
ae-TZ2P	−12.8	−12.6	−5.1	−4.8	−0.5	−0.2	23.1	23.5	−33.5	−33.0
ae-QZ4P	−13.3	−13.3	−5.3	−5.2	−0.8	−0.7	23.0	23.1	−33.4	−33.3
TZ2P ^c	−12.9	−12.7	−5.1	−4.9	−0.6	−0.4	23.1	23.4	−33.1	−32.7

^a Geometries optimized at ZORA-BLYP/TZ2P with frozen-core approximation, see Figure 1. ^b Relativistic effects treated with ZORA (see Section 2). ^c Standard frozen-core basis set (see Section 2.1).

basis set. The BSSE drops to 0.5 kcal/mol or less for this basis set and becomes even smaller, that is, 0.1 kcal/mol or less, if one goes to ae-QZ4P (see Table 5: the BSSE is the difference between “no CPC” and “with CPC” values). For example, the activation energy for the OxIn pathway, without counterpoise correction, varies from 1.9 to 0.3 to −0.5 to −0.8 kcal/mol along ae-DZ, ae-TZP, ae-TZ2P, and ae-QZ4P (Table 5, no CPC). The corresponding BSSE amounts to 3.4, 0.2, 0.3, and 0.1 kcal/mol (see Table 5). Note that, in fact, the BSSE is large, that is, a few kilocalories per mole, only for the smallest, ae-DZ, basis set. This is in line with our previous work on the oxidative addition of methane, ethane, and fluoromethane to Pd in which we found that basis-set convergence and elimination of the BSSE are achieved much earlier for DFT (e.g., B3LYP or BLYP) than for correlated ab initio methods [e.g., CCSD(T)].^{25–28} In general, correlated ab initio methods depend more strongly on the extent of polarization of the basis set because the polarization functions are essential to generate the configurations through which the wave function can describe the correlation hole. In DFT, on the other hand, the correlation hole is built into the potential and the energy functional and polarization functions mainly play the much less delicate role of describing polarization of the electron density. In conclusion, the TZ2P basis in combination with the frozen-core approximation yields an efficient and accurate (i.e., within 1 kcal/mol) description of the relative energies of our stationary points.

Finally, on the basis of the ZORA-BLYP/TZ2P geometries discussed above, we have computed the relative energies of stationary points along the PES for various LDA, GGA, meta-GGA, and hybrid functionals in combination with the all-electron ae-TZ2P basis set and ZORA for relativistic effects. This was done in a post-SCF manner, that is, using density functionals with the electron density obtained at ZORA-BLYP/ae-TZ2P. The performance of the density functionals is discussed by comparing the resulting potential energy surfaces with that of the ab initio [CCSD(T)] benchmark discussed above. The results of this survey are collected in Table 6, which shows energies relative to the separate reactants (R).

For clarity, we wish to point out that the above procedure for computing the relative energies shown in Table 6 differs in three respects from that used for computing the relative energies with the LDA functional and the seven GGA functionals shown in Table 4: (i) an all-electron approach is used instead of the frozen-core approximation; (ii) for all

density functionals, the BLYP optimized geometries are used instead of geometries optimized with the same functional, and (iii) for all functionals, the BLYP electron density is used for computing the energy instead of the electron density corresponding to that functional. The effect of going from frozen-core (TZ2P) to all-electron calculations (ae-TZ2P), that is, point i, is small, causing a stabilization of 0.3 kcal/mol or less, and has already been discussed above. The differences between the values in Tables 4 and 6 derive mainly from the combined effect of points ii and iii, which causes, considering the GGA functionals, a destabilization of up to 1.0 kcal/mol (for the PBE and OLYP transition state for the OxIn pathway) of the relative energies if one goes from Table 4 to Table 6. Both effects are on the order of a few tenths of a kilocalorie per mole up to maximally 1 kcal/mol and, for the different GGA functionals and stationary points, contribute to this destabilization with varying relative importance. For example, for TS_{OxIn}, the single-point approach contributes generally somewhat more (0.6–1.0 kcal/mol) to this destabilization than the post-SCF approach (up to 0.3 kcal/mol). This has been assessed by computing the relative energies of stationary points using approximation ii but not iii, that is, computing them with the electron density corresponding to the density functional under consideration but with the BLYP geometries; the resulting values are provided in parentheses in Table 6. In conclusion, for the GGA functionals, the combined effect of approximations i–iii on the relative energies of stationary points is on the order of a few tenths of a kilocalorie per mole with an upper limit of 1 kcal/mol.

Now, we extend our survey to the full range of energy density functionals that, except for LDA and the seven GGAs discussed above, have been implemented in the ADF program in a post-SCF manner. For all 26 density functionals, we have computed the mean absolute error in the relative energies of the reactant complexes, transition states, and product and the error in the barriers, that is, the relative energy of the transition states, as compared with the CCSD(T) benchmark (see Table 6). In Section 3.2, we have pointed out that the CCSD(T) relative energy for the S_N2 transition state TS_{S_N2-ra} is unreliable and must be treated with great precaution. Indeed, for this particular species, the counterpoise-corrected CCSD(T)/BS5 value of the relative energy exceeds the corresponding values obtained with the various density functionals to an unusually great extent, even those which normally overestimate this type of reaction

Table 6. Energies (in kcal/mol) Relative to the Separate Reactants (R) of the Stationary Points^a along the Reaction Coordinates of the OxIn- and S_N2-type Pathways for Oxidative Addition of the C–Cl Bond of CH₃Cl to Pd and Dissociation Energy of CH₃Cl into a Methyl Radical and Chlorine Atom (*D*_{CCl}), Computed for 26 Different Density Functionals with the ae-TZ2P Basis Set with All Electrons Treated Variationally,^b and Compared to the ab Initio Benchmark from This Work.

method	RC _{OxIn}	RC _{S_N2}	TS _{OxIn}	TS _{S_N2-ra}	P	mean abs. err. ^c	mean abs. err., excl. TS _{S_N2-ra} ^d	err. in OxIn barr. ^c	err. in S _N 2-ra barr. ^c	<i>D</i> _{CCl}	err. in <i>D</i> _{CCl} ^e
LDA											
VWN	−27.6 (−27.7)	−20.7 (−21.0)	−18.2 (−18.4)	18.7 (7.7)	−50.2 (−50.3)	20.1	19.0	−22.0	−24.6	106.2	25.0
GGA											
BP86	−16.0 (−16.0)	−8.6 (−8.7)	−4.5 (−4.5)	23.8 (23.8)	−37.0 (−37.0)	9.0	6.3	−8.3	−19.5	86.0	4.9
BLYP	−12.8	−5.1	−0.5	23.1	−33.5	6.4	2.9	−4.2	−20.2	82.1	1.0
B88xBR89c	−13.9	−5.8	−0.4	22.6	−35.9	7.2	3.8	−4.2	−20.7	83.4	2.2
PW91	−17.2 (−17.2)	−10.1 (−10.1)	−5.8 (−5.8)	23.0 (23.1)	−38.0 (−37.9)	10.1	7.6	−9.6	−20.3	88.9	7.7
PBE	−16.4 (−16.6)	−9.5 (−9.6)	−5.1 (−5.1)	23.6 (23.7)	−37.2 (−37.1)	9.4	6.9	−8.9	−19.7	88.9	7.7
FT97	−12.7	−10.5	3.8	23.5	−36.9	7.1	3.9	0.0	−19.8	84.7	3.5
revPBE	−11.6 (−11.8)	−4.6 (−4.8)	0.7 (0.7)	26.3 (26.2)	−31.7 (−31.7)	5.0	2.0	−3.1	−17.0	83.5	2.4
HCTH/93	−6.6	0.4	8.0	32.1	−22.7	6.2	4.9	4.2	−11.2	83.0	1.9
RPBE	−11.1 (−11.3)	−4.1 (−4.3)	1.4 (1.3)	26.3 (26.2)	−30.9 (−30.9)	4.7	1.7	−2.4	−17.0	82.9	1.8
BOP	−9.6	−1.9	3.4	25.4	−29.9	5.0	1.8	−0.3	−17.9	81.8	0.6
HCTH/120	−11.0	−3.9	3.0	28.5	−27.5	3.6	0.8	−0.8	−14.8	84.3	3.2
HCTH/147	−10.4	−3.3	3.6	29.1	−27.0	3.7	1.0	−0.2	−14.2	84.3	3.1
HCTH/407	−7.8	−1.3	8.0	30.8	−22.7	5.9	4.2	4.2	−12.4	83.2	2.1
OLYP	−6.0 (−6.5)	0.7 (0.2)	8.0 (7.7)	31.9 (31.3)	−23.3 (−23.7)	6.3	5.0	4.2	−11.4	83.6	2.4
Meta-GGA											
BLAP3	−7.7	0.2	7.5	27.7	−26.7	5.9	3.5	3.7	−15.6	85.3	4.1
VS98	−14.2	−8.9	−5.7	25.7	−33.5	7.8	5.4	−9.5	−17.6	81.2	0.1
KCIS	−13.7	−6.7	−1.6	26.0	−34.7	6.6	4.0	−5.4	−17.3	85.4	4.2
PKZB	−12.5	−5.2	−0.5	26.6	−34.4	5.8	3.0	−4.3	−16.7	83.6	2.5
Bmr1	−7.4	0.5	7.9	27.3	−26.4	6.2	3.8	4.1	−16.0	83.7	2.5
OLAP3	−0.9	6.1	16.0	36.5	−16.5	10.4	11.3	12.2	−6.8	86.8	5.6
TPSS	−14.4	−6.7	−3.7	25.0	−36.9	7.9	5.3	−7.5	−18.3	84.2	3.0
Hybrid											
B3LYP	−9.3	−3.1	5.4	36.3	−26.5	2.8	1.8	1.6	−7.0	81.2	0.1
O3LYP	−5.4	0.5	10.1	40.4	−19.6	5.9	6.6	6.3	−2.9	85.7	4.5
X3LYP	−9.7	−3.7	5.0	36.9	−26.7	2.4	1.4	1.2	−6.3	81.7	0.6
TPSSh	−12.3	−5.4	−0.3	31.6	−32.9	4.4	2.6	−4.1	−11.7	83.2	2.0
Ab Initio Benchmark (This Work) ^f											
CCSD(T)	−11.2	−5.4	3.8	(43.3) ^g	−28.0					81.2	

^a Geometries optimized at ZORA-BLYP/TZ2P with frozen-core approximation, see Figure 1. ^b Computed post-SCF using the BLYP electron density, unless stated otherwise. Values in parentheses computed self-consistently, i.e., with the potential and electron-density corresponding to the energy functional indicated. Relativistic effects treated with ZORA (see Section 2). ^c Mean absolute error for the energies of the five stationary points RC_{OxIn}, RC_{S_N2}, TS_{OxIn}, TS_{S_N2-ra}, and P relative to the separate reactants (R) and error in the overall barriers, i.e., in the energy of TS_{OxIn} and TS_{S_N2-ra}, respectively, relative to R, compared with the CCSD(T) benchmark from this work. ^d Mean absolute error corresponding to footnote c but excluding stationary point TS_{S_N2-ra}. ^e Error in the dissociation energy of the C–Cl bond in chloromethane, compared with the CCSD(T) benchmark from this work. ^f CCSD(T) benchmark from this work, based on BLYP-optimized geometries. ^g CCSD(T) procedure not reliable for C–Cl S_N2 transition state, see Section 3.2.

barrier, such as OLYP (see Table 6). For comparison, deviations of the DFT barriers are significantly smaller for the transition state of the OxIn pathway, and they also show the well-known scattering of individual values somewhat above and below the CCSD(T) benchmark value. Thus, for all density functionals except O3LYP, the mean absolute error between the DFT and CCSD(T) relative energies of the stationary points along the OxIn and S_N2 PESs drops significantly if one excludes the S_N2-ra transition state; Table 6 displays both values in the columns “mean abs. err.” and “mean abs. err. excl. TS_{S_N2-ra}”. In the following, we discuss the latter. Both the mean absolute error and the error in the OxIn barrier drop significantly if one goes from LDA (mean absolute error = 19.0 kcal/mol), which, as mentioned above, suffers from its infamous overbinding, to GGA functionals

(mean absolute error = 0.8–7.6 kcal/mol). However, no significant improvement occurs if one goes from GGA to the more recently developed meta-GGA functionals (mean absolute error = 3.0–11.3 kcal/mol) and hybrid functionals (mean absolute error = 1.4–6.6 kcal/mol). The best overall agreement with the ab initio benchmark PES is achieved by functionals of the GGA (HCTH/120), meta-GGA (PKZB), and hybrid DFT type (X3LYP), with mean absolute errors of 0.8–3.0 kcal/mol and errors in the OxIn barrier ranging from −4.3 to 1.2 kcal/mol. Interestingly, the well-known BLYP functional compares very reasonably with an only slightly larger mean absolute error of 2.9 kcal/mol and an underestimation of the OxIn barrier of −4.2 kcal/mol. The OLYP functional overestimates the OxIn barrier by the same amount, 4.2 kcal/mol, but has a larger mean absolute error

Table 7. Relative Energies (in kcal/mol) of the Stationary Points along the Reaction Coordinate for the Oxidative Addition of Pd to the C–H, C–C, C–F, and C–Cl Bonds, Computed with CCSD(T), BLYP, OLYP, and B3LYP^a

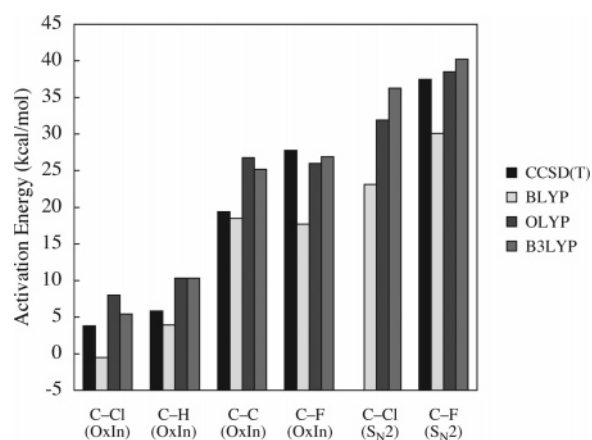
activated bond		reactant complex				transition state				product			
		CCSD(T)	BLYP	OLYP	B3LYP	CCSD(T)	BLYP	OLYP	B3LYP	CCSD(T)	BLYP	OLYP	B3LYP
C–H	OxIn	–8.1	–6.7	–0.7	–4.9	5.8	3.9	10.3	10.3	0.8	–3.6	5.3	4.6
C–C	OxIn	–10.8	–6.7	–0.5	–4.9	19.4	18.5	26.8	25.2	–4.5	–9.5	1.6	0.2
C–F	OxIn					27.8	17.7	26.0	26.9				
	S _N 2	–5.3	–5.4	0.3	–3.4	37.5	30.1	38.5	40.2	–6.4	–16.3	–6.2	–7.0
C–Cl	OxIn	–11.2	–12.8	–6.0	–9.3	3.8	–0.5	8.0	5.4				
	S _N 2	–5.4	–5.1	0.7	–3.1	(43.3) ^b	23.1	31.9	36.3	–28.0	–33.5	–23.3	–26.5

^a Geometries optimized at ZORA-BLYP/TZ2P with frozen-core approximation. BLYP, OLYP, and B3LYP results calculated with the ae-TZ2P basis set with all electrons treated variationally and post-SCF using the BLYP electron density. CCSD(T) results calculated with relativistic four-component method. For details, see refs 25, 26 (C–H), 27 (C–C), 28 (C–F), and this work (C–Cl). ^b CCSD(T) procedure not reliable for C–Cl S_N2 transition state, see Section 3.2.

of 5.0 kcal/mol (in the case of C–F bond activation,²⁸ OLYP performs better than BLYP). The hybrid functionals B3LYP and X3LYP perform remarkably well, with overestimations of the barrier of only 1.6 and 1.2 kcal/mol and mean absolute errors of only 1.8 and 1.4 kcal/mol, respectively.

We have verified to what extent errors made, for example, by BLYP or B3LYP, originate from a failure in describing the C–Cl bond dissociation. To this end, we have first computed an ab initio benchmark for the C–Cl bond strength, that is, the dissociation energy D_{CCl} , associated with the reaction $\text{H}_3\text{C–Cl} \rightarrow \text{CH}_3^\bullet + \text{Cl}^\bullet$ at the same levels of theory as we did for the PES of the oxidative addition of the chloromethane C–Cl bond to Pd. This was done again using the BLYP-optimized geometries, which yield a C–H bond length of 1.084 Å for the D_{3h} symmetric methyl radical. Thus, we arrive at a dissociation energy of 81.2 kcal/mol at CCSD(T) with basis set BS5 and with counterpoise correction (HF, 60.0; MP2, 86.0; and CCSD, 78.2 kcal/mol; for details, see Table S5 in the Supporting Information), in nice agreement with the experimental value for the enthalpy at 0 K, namely, 82.04 ± 0.26 kcal/mol.⁸⁹ Most functionals are able to describe the dissociation energy reasonably well, yielding errors, compared with the CCSD(T) benchmark, on the order of a few kilocalories per mole. For BLYP and B3LYP, the dissociation energy D_{CCl} is overestimated by only 1.0 and 0.1 kcal/mol, respectively (see Table 6). In conclusion, the underestimation of the activation energy by BLYP cannot be ascribed to a failure in describing C–Cl bond dissociation (in fact, the slight error in the latter works in the opposite direction and should raise the value of the barrier). Rather, it may be related to the overbinding between Pd and the methyl and chloride ligands (compare relative energies for P in Table 6).

3.4. Comparison of C–H, C–C, C–F, and C–Cl Bond Activation. Finally, we have carried out a comprehensive comparison of the ab initio CCSD(T) benchmark PESs as well as the corresponding BLYP, OLYP, and B3LYP density functional results for the palladium-induced activation of methane C–H (OxIn),^{25,26} ethane C–C (OxIn),²⁷ fluoromethane C–F (OxIn and S_N2),²⁸ and the C–Cl bond (this work, OxIn and S_N2) using the same computational details throughout. The energies of all stationary points relative to the reactants are collected in Table 7. Trends in activation energies are graphically displayed in Figure 3 in which the

**Figure 3.** Activation energies (in kcal/mol) for the oxidative addition of Pd to various C–X bonds, computed with CCSD(T), BLYP, OLYP, and B3LYP. For computational details, see the footnotes of Table 7.

questionable CCSD(T) value for the S_N2 transition state for C–Cl activation has been left out (see also Section 3.2).

It is clear, especially from Figure 3, that all important features of the CCSD(T) benchmark potential energy surfaces for palladium-induced C–H, C–C, C–F, and C–Cl bond activation are reproduced by important functionals such as BLYP, OLYP, and B3LYP. On the other hand, a more detailed look also shows that none of these functionals is the “best one” for each individual model reaction. For example, BLYP performs best in the case of C–H and C–C bond activation whereas OLYP and B3LYP overestimate the barrier (compare values in Table 7). But, in the case of C–F bond activation, the BLYP functional underestimates the barriers of both OxIn and S_N2 pathways while OLYP and B3LYP perform very satisfactorily [Table 7, OxIn pathway: CCSD(T), 27.8 kcal/mol; BLYP, 17.7 kcal/mol; OLYP, 26.0 kcal/mol; B3LYP, 26.9 kcal/mol; S_N2-pathway: CCSD(T), 37.5 kcal/mol; BLYP, 30.1 kcal/mol; OLYP, 38.5 kcal/mol; B3LYP, 40.2 kcal/mol]. For the C–Cl bond, as described above, the OxIn barrier is only slightly underestimated by BLYP and overestimated by OLYP and B3LYP. Nevertheless, they all agree with the CCSD(T) benchmark that, for example, the activation energies for oxidative addition increase in the order C–Cl (OxIn) < C–H (OxIn) < C–C (OxIn) ≤ C–F (OxIn) < C–Cl (S_N2-ra; no reliable benchmark) < C–F (via S_N2-ra), see Figure 3.

4. Conclusions

We have computed an ab initio benchmark for the archetypal oxidative addition of the chloromethane C–Cl bond to palladium that derives from a hierarchical series of relativistic methods and highly polarized basis sets for the palladium atom, up to the counterpoise corrected, four-component spin-free Dirac-Coulomb CCSD(T)/(24s16p13d+4f+p+g) level, which is converged with respect to the basis-set size within 1 kcal/mol. Our findings stress the importance of sufficient higher-angular momentum polarization functions, f and g, as well as counterpoise correction for obtaining reliable activation energies.

This benchmark is used to evaluate the performance of 26 relativistic (ZORA) density functionals for describing relative energies of stationary points on the potential energy surface. Excellent agreement with our ab initio benchmark for energies relative to the reactants is achieved by functionals of the GGA, meta-GGA, and hybrid DFT approaches, each of which have a representative in the top three, with mean absolute errors as small as 3.0 kcal/mol or less. All theoretical methods used reveal the existence of two possible reaction mechanisms for oxidative addition: direct oxidative insertion (OxIn) with a barrier that is at least some 20 kcal/mol lower than that of an alternative S_N2 pathway. Interestingly, the well-known BLYP functional still performs satisfactorily with a mean absolute error of 2.9 kcal/mol and an underestimation of the OxIn barrier by -4.2 kcal/mol. Note that the much advocated B3LYP hybrid functional also performs remarkably well, with a mean absolute error of 1.8 kcal/mol and an overestimation of the OxIn barrier by only 1.6 kcal/mol.

Finally, a comprehensive comparison of the present (C–Cl) and previous studies^{25–28} shows that all important features of the CCSD(T) benchmark potential energy surfaces for palladium-induced C–H, C–C, C–F, and C–Cl bond activation are reproduced by important functionals such as BLYP, OLYP, and B3LYP. Thus, while none of these functionals is the “best one” for each individual model reaction, they all agree with the CCSD(T) benchmark that, for example, the activation energies for oxidative addition increase in the order C–Cl (OxIn) < C–H (OxIn) < C–C (OxIn) \lesssim C–F (OxIn) < C–Cl (S_N2 -ra; no reliable benchmark) < C–F (via S_N2 -ra). Our DFT results have been verified to be converged with the basis-set size at ZORA-BLYP/TZ2P and to be unaffected by the frozen-core approximation for the core shells of carbon (1s), chlorine (1s2s2p), and palladium (1s2s2p3s3p3d). We consider this a sound and efficient approach for the routine investigation of catalytic bond activation, also in larger, more realistic model systems.

Acknowledgment. We thank the Nederlandse Organisatie voor Wetenschappelijk Onderzoek (NWO-CW and NWO-NCF) for financial support. We thank Ivan Infante for helpful discussions.

Supporting Information Available: Structures of stationary points optimized with LDA and various GGA functionals, total energy and BSSE of all stationary points

involved at all levels of ab initio theory applied in the computations, and reaction profiles obtained with CCSD(T) and various GGA functionals. This material is available free of charge via the Internet at <http://pubs.acs.org>.

References

- (1) Frisch, A. C.; Beller, M. *Angew. Chem.* **2005**, *117*, 680.
- (2) Senn, H. M.; Ziegler, T. *Organometallics* **2004**, *23*, 2980.
- (3) Bickelhaupt, F. M.; Ziegler, T.; von Ragué Schleyer, P. *Organometallics* **1995**, *14*, 2288.
- (4) Albert, K.; Gisdakis, P.; Rösch, N. *Organometallics* **1998**, *17*, 1608.
- (5) Sundermann, A.; Uzan, O.; Martin, J. M. L. *Chem.—Eur. J.* **2001**, *7*, 1703.
- (6) Diefenbach, A.; Bickelhaupt, F. M. *J. Chem. Phys.* **2001**, *115*, 4030.
- (7) Smurnyi, E. D.; Gloriov, I. P.; Ustynuk, Y. A. *Russ. J. Phys. Chem.* **2003**, *77*, 1699.
- (8) Reinhold, M.; McGrady, J. E.; Perutz, R. N. *J. Am. Chem. Soc.* **2004**, *126*, 5268.
- (9) Diefenbach, A.; Bickelhaupt, F. M. *J. Phys. Chem. A* **2004**, *108*, 8460.
- (10) Diefenbach, A.; de Jong, G. Th.; Bickelhaupt, F. M. *J. Chem. Theory Comput.* **2005**, *1*, 286.
- (11) Diefenbach, A.; de Jong, G. Th.; Bickelhaupt, F. M. *Mol. Phys.* **2005**, *103*, 995.
- (12) Dedieu, A. *Chem. Rev.* **2000**, *100*, 543.
- (13) Kiplinger, J. L.; Richmond, T. G.; Osterberg, C. E. *Chem. Rev.* **1994**, *94*, 373.
- (14) Møller, C.; Plesset, M. S. *Phys. Rev.* **1934**, *46*, 618.
- (15) Cizek, J. *J. Chem. Phys.* **1966**, *45*, 4256.
- (16) Purvis, G. D., III; Bartlett, R. J. *J. Chem. Phys.* **1982**, *76*, 1910.
- (17) Raghavachari, K.; Trucks, G. W.; Pople, J. A.; Head-Gordon, M. *Chem. Phys. Lett.* **1989**, *157*, 479.
- (18) Boys, S. F.; Bernardi, F. *Mol. Phys.* **1970**, *19*, 553.
- (19) Baker, J.; Muir, M.; Andzelm, J. J. *J. Chem. Phys.* **1995**, *102*, 2063.
- (20) Barone, V.; Adamo, C. *J. Chem. Phys.* **1996**, *105*, 11007.
- (21) Thümmel, H. T.; Bauschlicher, C. W., Jr. *J. Phys. Chem. A* **1997**, *101*, 1188.
- (22) Bach, R. D.; Glukhovtsev, M. N.; Gonzales, C. *J. Am. Chem. Soc.* **1998**, *120*, 9902.
- (23) Gritsenko, O. V.; Ensing, B.; Schippers, P. R. T.; Baerends, E. J. *J. Phys. Chem. A* **2000**, *104*, 8558.
- (24) Poater, J.; Solà, M.; Duran, M.; Robles, J. *J. Phys. Chem. Chem. Phys.* **2002**, *4*, 722.
- (25) de Jong, G. Th.; Solà, M.; Visscher, L.; Bickelhaupt, F. M. *J. Chem. Phys.* **2004**, *121*, 9982.
- (26) de Jong, G. Th.; Geerke, D. P.; Diefenbach, A.; Bickelhaupt, F. M. *J. Chem. Phys.* **2005**, *123*, 261.
- (27) de Jong, G. Th.; Geerke, D. P.; Diefenbach, A.; Solà, M.; Bickelhaupt, F. M. *J. Comput. Chem.* **2005**, *26*, 1006.
- (28) de Jong, G. Th.; Bickelhaupt, F. M. *J. Phys. Chem. A* **2005**, *109*, 9685.

- (29) Hohenberg, P.; Kohn, W. *Phys. Rev.* **1964**, *136*, B864.
- (30) Kohn, W.; Sham, L. J. *Phys. Rev.* **1965**, *140*, A1133.
- (31) Parr, R. G.; Yang, W. *Density-Functional Theory of Atoms and Molecules*; Oxford University Press: New York, 1989.
- (32) Baerends, E. J.; Ellis, D. E.; Ros, P. *Chem. Phys.* **1973**, *2*, 41.
- (33) Fonseca Guerra, C.; Snijders, J. G.; te Velde, G.; Baerends, E. J. *Theor. Chem. Acc.* **1998**, *99*, 391.
- (34) te Velde, G.; Bickelhaupt, F. M.; Baerends, E. J.; Fonseca Guerra, C.; van Gisbergen, S. J. A.; Snijders, J. G.; Ziegler, T. *J. Comput. Chem.* **2001**, *22*, 931.
- (35) Baerends, E. J.; Autschbach, J. A.; Bérces, A.; Bo, C.; Boerrigter, P. M.; Cavallo, L.; Chong, D. P.; Deng, L.; Dickson, R. M.; Ellis, D. E.; Fan, L.; Fischer, T. H.; Fonseca Guerra, C.; van Gisbergen, S. J. A.; Groeneveld, J. A.; Gritsenko, O. V.; Grüning, M.; Harris, F. E.; van den Hoek, P.; Jacobsen, H.; van Kessel, G.; Kootstra, F.; van Lenthe, E.; Osinga, V. P.; Patchkovskii, S.; Philipsen, P. H. T.; Post, D.; Pye, C. C.; Ravenek, W.; Ros, P.; Schipper, P. R. T.; Schreckenbach, G.; Snijders, J. G.; Sola, M.; Swart, M.; Swerhone, D.; te Velde, G.; Vernooijs, P.; Versluis, L.; Visser, O.; van Wezenbeek, E.; Wiesenekker, G.; Wolff, S. K.; Woo, T. K.; Ziegler, T. *ADF2002.03*; SCM, Theoretical Chemistry, Vrije Universiteit: Amsterdam, The Netherlands, 2002.
- (36) Vosko, S. H.; Wilk, L.; Nusair, M. *Can. J. Phys.* **1980**, *58*, 1200.
- (37) Becke, A. D. *Phys. Rev. A* **1988**, *38*, 3098.
- (38) Perdew, J. P. *Phys. Rev. B* **1986**, *33*, 8822.
- (39) Lee, C.; Yang, W.; Parr, R. G. *Phys. Rev. B* **1988**, *37*, 785.
- (40) Perdew, J. P. In *Electronic Structure of Solids '91*; Ziesche, P., Eschrig, H., Eds.; Akademie Verlag: Berlin, 1991.
- (41) Perdew, J. P.; Wang, Y. *Phys. Rev. B* **1992**, *45*, 13244.
- (42) Perdew, J. P.; Chevary, J. A.; Vosko, S. H.; Jackson, K. A.; Pederson, M. R.; Singh, D. J.; Fiolhais, C. *Phys. Rev. B* **1992**, *46*, 6671.
- (43) Perdew, J. P.; Chevary, J. A.; Vosko, S. H.; Jackson, K. A.; Pederson, M. R.; Singh, D. J.; Fiolhais, C. *Phys. Rev. B* **1993**, *49*, 4978(E).
- (44) Perdew, J. P.; Burke, K.; Ernzerhof, M. *Phys. Rev. Lett.* **1996**, *77*, 3865.
- (45) Perdew, J. P.; Burke, K.; Ernzerhof, M. *Phys. Rev. Lett.* **1997**, *78*, 1396(E).
- (46) Zhang, Y.; Yang, W. *Phys. Rev. Lett.* **1998**, *80*, 890.
- (47) Hammer, B.; Hansen, L. B.; Nørkov, J. K. *Phys. Rev. B* **1999**, *59*, 7413.
- (48) Handy, N. C.; Cohen, A. J. *Mol. Phys.* **2001**, *99*, 403.
- (49) van Lenthe, E.; Baerends, E. J.; Snijders, J. G. *J. Chem. Phys.* **1994**, *101*, 9783.
- (50) Visscher, L.; Lee, T. J.; Dyal, K. G. *J. Chem. Phys.* **1996**, *105*, 8769.
- (51) Jensen, H. J. A.; Saue, T.; Visscher, L. *DIRAC*, release 4.0; Syddansk Universitet: Odense, Denmark, 2004.
- (52) Dyal, K. G. *J. Chem. Phys.* **1994**, *100*, 2118.
- (53) Visscher, L. *Theor. Chem. Acc.* **1997**, *98*, 68.
- (54) Dunning, T. H., Jr. *J. Chem. Phys.* **1989**, *90*, 1007.
- (55) Kendall, R. A.; Dunning, T. H., Jr.; Harrison, R. J. *J. Chem. Phys.* **1992**, *96*, 6796.
- (56) Visscher, L.; Aerts, P. J. C.; Visser, O.; Nieuwpoort, W. C. *Int. J. Quantum Chem.* **1991**, *25*, 131.
- (57) Ehlers, A. W.; Böhme, M.; Dapprich, S.; Gobbi, A.; Höllwarth, A.; Jonas, V.; Köhler, K. F.; Stegmann, R.; Veldkamp, A.; Frenking, G. *Chem. Phys. Lett.* **1993**, *208*, 111.
- (58) Langhoff, S. R.; Petterson, L. G. M.; Bauschlicher, C. W., Jr. *J. Chem. Phys.* **1987**, *86*, 268.
- (59) Osanai, Y.; Sekiya, M.; Noro, T.; Koga, T. *Mol. Phys.* **2003**, *101*, 65.
- (60) Becke, A. D. *J. Chem. Phys.* **1988**, *88*, 1053.
- (61) Becke, A. D.; Roussel, M. R. *Phys. Rev. A* **1989**, *39*, 3761.
- (62) Filatov, M.; Thiel, W. *Mol. Phys.* **1997**, *91*, 847.
- (63) Hamprecht, F. A.; Cohen, A. J.; Tozer, D. J.; Handy, N. C. *J. Chem. Phys.* **1998**, *109*, 6264.
- (64) Tsuneda, T.; Suzumura, T.; Hirao, K. *J. Chem. Phys.* **1999**, *110*, 10664.
- (65) Boese, A. D.; Doltsinis, N. L.; Handy, N. C.; Sprik, M. *J. Chem. Phys.* **2000**, *112*, 1670.
- (66) Boese, A. D.; Handy, N. C. *J. Chem. Phys.* **2001**, *114*, 5497.
- (67) Proynov, E. I.; Sirois, S.; Salahub, D. R. *Int. J. Quantum Chem.* **1997**, *64*, 427.
- (68) van Voorhis, T.; Scuseria, G. E. *J. Chem. Phys.* **1998**, *109*, 400.
- (69) Krieger, J. B.; Chen, J.; Iafrate, G. J.; Savin, A. In *Electron Correlation and Material Properties*; Gonis, A., Kioussis, N., Eds.; Plenum: New York, 1999.
- (70) Perdew, J. P.; Kurth, S.; Zupan, A.; Blaha, P. *Phys. Rev. Lett.* **1999**, *82*, 2544.
- (71) Perdew, J. P.; Kurth, S.; Zupan, A.; Blaha, P. *Phys. Rev. Lett.* **1999**, *82*, 5179(E).
- (72) Proynov, E.; Chermette, H.; Salahub, D. R. *J. Chem. Phys.* **2000**, *113*, 10013.
- (73) Tao, J.; Perdew, J. P.; Staroverov, V. N.; Scuseria, G. E. *Phys. Rev. Lett.* **2003**, *91*, 146401.
- (74) Staroverov, V. N.; Scuseria, G. E.; Tao, J.; Perdew, J. P. *J. Chem. Phys.* **2003**, *119*, 12129.
- (75) Becke, A. D. *J. Chem. Phys.* **1993**, *98*, 5648.
- (76) Stephens, P. J.; Devlin, F. J.; Chabalowski, C. F.; Frisch, M. J. *J. Phys. Chem.* **1994**, *98*, 11623.
- (77) Cohen, A. J.; Handy, N. C. *Mol. Phys.* **2001**, *99*, 607.
- (78) Xu, X.; Goddard, W. A., III. *Proc. Natl. Acad. Sci. U.S.A.* **2004**, *101*, 2673.
- (79) Hertwig, R. H.; Koch, W. *Chem. Phys. Lett.* **1997**, *268*, 345.
- (80) Frenking, G.; Antes, I.; Böhme, M.; Dapprich, S.; Ehlers, A. W.; Jonas, V.; Neuhaus, A.; Otto, M.; Stegmann, R.; Veldkamp, A.; Vyboishchikov, S. F. Pseudopotential calculations of transition metal compounds. In *Reviews in*

- Computational Chemistry*; Lipkowitz, K. B., Boyd, D. B., Eds.; VCH Publishers Inc.: New York, 1996; Vol. 8, p 63.
- (81) Cundari, T. R.; Benson, M. T.; Lutz, M. L. Effective core potential approaches to the chemistry of heavier elements. In *Reviews in Computational Chemistry*; Lipkowitz, K. B., Boyd, D. B., Eds.; VCH Publishers Inc.: New York, 1996; Vol. 8, p 145.
- (82) Hay, P. J.; Wadt, W. R. *J. Chem. Phys.* **1985**, 82, 299.
- (83) Jonas, V.; Frenking, G.; Reetz, M. T. *J. Comput. Chem.* **1992**, 13, 919.
- (84) Our computational resources do not allow for larger basis sets than BS3 in the case of the $\text{PdCl}^- + \text{CH}_3\text{Cl}$ model reaction system. This basis set should, however, yield relative energies that are reasonably converged with basis-set size, as can be seen for other stationary points in Table 2.
- (85) Counterpoise-corrected relative energies of transition state $\text{TS}_{\text{S}_{\text{N}}2-\text{ra}}$ of $\text{PdCl}^- + \text{CH}_3\text{Cl}$ are -10.2 , -13.8 , -17.7 , and -18.8 kcal/mol at HF, MP2, CCSD, and CCSD(T), respectively, in combination with basis set BS3. For details, see Table S4 in the Supporting Information.
- (86) Nibbering, N. M. M. *Adv. Phys. Org. Chem.* **1988**, 24, 1.
- (87) Carroll, J. J.; Weisshaar, J. C. *J. Am. Chem. Soc.* **1993**, 115, 800.
- (88) Bickelhaupt, F. M. *Mass Spectrom. Rev.* **2001**, 20, 347.
- (89) Johnson, R. D., III. NIST Computational Chemistry Comparison and Benchmark Database, NIST Standard Reference Database Number 101, Release 11. <http://srdata.nist.gov/cccbdb> (accessed June 2005).

CT050254G